RSC Advances

PAPER

View Article Online
View Journal | View Issue

Cite this: *RSC Adv.*, 2020, **10**, 42432

Cheap, facile, and upscalable activated carbon-based photothermal layers for solar steam generation†

Anush Mnoyan,‡[a] Myeongil Choi,‡[a] Dong Hyun Kim,[a] Bon-Jun Ku,[a] Hyunjoung Kim,[a] Kyung Jin Lee,[b] Ahmed S. Yasin,[a] Sungchan Nam*[c] and Kyubock Lee*[a]

Solar-to-steam generation characterized by nanostructured photothermal materials and interfacial heating is developed based on various carbon nanostructures such as graphene, reduced graphene oxide, CNT, or their combinations. However, multiple and sophisticated synthetic steps are required to generate macroscopic porosity in photothermal devices for the efficient mass transport of water and generated steam. Additionally, the fabrication of photothermal layers on a practical scale constitutes the main hurdle for real applications toward solar-driven desalination. Herein, we report on the development of highly efficient photothermal layers with a commercially available low-cost material, activated carbon (AC), by using facile filtration and spray coating methods, which lead to the generation of intraparticle porous structure without any additional processing. The AC-based photothermal layers generated 1.17 kg m^{-2} h^{-1} of steam under 1 sun, and 4.7 wt% of polyethyleneimine coating on AC enhanced steam generation by 8.5% under 1 sun, corresponding to 1.27 kg m^{-2} h^{-1} of the water evaporation rate and 85.66% of the photothermal conversion efficiency. This was due to improvements in light absorption and water uptake properties with the additional advantage of mechanical robustness. The outdoor solar-to-steam generation test with the spray-coated A4-sized photothermal layer in conjunction with the desalination test demonstrated the potential for practical desalination application with upscalability.

Received 9th September 2020
Accepted 2nd November 2020

DOI: 10.1039/d0ra07746a

rsc.li/rsc-advances

1. Introduction

Various technologies involving photovoltaic power generation, photocatalytic water splitting, and solar desalination can be applied for the efficient exploitation of abundant and clean solar energy, and this is becoming crucial for the sustainable development of human society.[1–3] Specifically, solar desalination is attractive in areas with water scarcity and high solar irradiation. Conventional solar desalination involves collecting solar energy by means of mirrors or lenses that track the motion of the sun, and it is developed and applied for producing freshwater for decades. However, low efficiency originating from heating bulk water, heat loss, and high construction cost limits the utilization of solar desalination to less than 1% of worldwide desalination.[4]

A new approach to solar desalination is recently introduced. The approach is characterized by solar thermal conversion using nanostructured photothermal materials and steam generation through interfacial water heating.[5] Given that the heating occurs locally at the interface of photothermal layer and thin water film instead of in bulk water, 1 sun under ambient conditions is sufficient for steam generation with very high efficiency. The key factors required for high efficiency steam generation using the photothermal layer are broadband light absorption and high wettability of water. Additionally, cost effectiveness and feasibility of scaling up are inevitable for practical applications. The most widely utilized photothermal materials for steam generation are metal-based plasmonic nanomaterials (NPs),[5–9] carbon materials with blackbody effect,[10–22] and other materials such as metal oxides, polymers[23–27] or even natural materials.[28] The narrow absorptivity of the subwavelength plasmonic NPs in visible light limits efficient energy utilization over the entire solar spectrum.[29,30] Furthermore, high cost makes them less attractive for wide applications. Carbon-based materials, which are relatively cheap and show intense absorption throughout the entire solar spectrum, are able to achieve higher absorptivity when compared to plasmonic NPs and are considered as the most promising

[a]*Graduate School of Energy Science and Technology, Chungnam National University, 99 Daehak-ro, Yuseong-gu, Daejeon, 34134, Republic of Korea. E-mail: kyubock.lee@cnu.ac.kr; Tel: +82-42-821-8610*

[b]*Department of Chemical Engineering and Applied Chemistry, College of Engineering, Chungnam National University, 99 Daehak-ro, Yuseong-gu, Daejeon, 34134, Republic of Korea*

[c]*Greenhouse Gas Research Laboratory, Korea Institute of Energy Research, 152 Gajeong-ro, Yuseong-gu, Daejeon, 34129, Republic of Korea. E-mail: scnam@kier.re.kr*

† Electronic supplementary information (ESI) available. See DOI: 10.1039/d0ra07746a

‡ The first two authors contributed equally to this paper.

photothermal conversion materials.[13] Specifically, various carbon nanomaterials, such as graphene, reduced graphene oxide (rGO), CNT or their combinations, are applied for the development of solar-to-steam generators with high photothermal conversion properties.[11,14–18,20] Recent studies show that the steam generation efficiency can be significantly enhanced by rationally designing structures of reservoirs and photothermal layers for efficient energy managements.[31–33]

In the preparation of a photothermal layer using the aforementioned carbon nanomaterials, various synthetic approaches are introduced to generate monolithic open macropore channels through which water is transported by capillary action and generated steam escapes.[11,15,16,18,20,22] In the absence of macropore channels, the densely packed layer of carbon nanostructure easily retards such mass transport and steam generation. For example, Shi *et al.* fabricated rGO-based porous photothermal layer and obtained a water evaporation rate corresponding to 1.31 kg m^{-2} h^{-1} under illumination of 1 sun using the photothermal layer with optimized porosity. They controlled the porosity by introducing and removing sacrificing templates of SBA-15 particles.[18] Hu and co-workers used layer-by-layer 3D-printing technique to construct a porous all-in-one steam generator that included three layers, namely a CNT/graphene oxide (GO) film, GO/nano-fibrillated cellulose (NFC) mesh, and GO/NFC wall for high solar absorption, efficient water transportation, and thermal insulation, respectively. They reported a water evaporation rate of 1.25 kg m^{-2} h^{-1} under illumination of 1 sun.[15] Another type of 3D-structured porous graphene steam generator was fabricated *via* chemical vapor deposition growth of N-doped graphene on bicontinuous porous Ni template, and this was followed by removing the template, thereby resulting in a water evaporation rate of 1.5 kg m^{-2} h^{-1} under illumination of 1 sun.[11] However, the fabrication methods of carbon-based photothermal layers with monolithic open macropore channels require several processing steps, high material cost, and are typically restricted to small scale, thereby making their practical application infeasible.

Herein, we devised a cheap, facile, and upscalable solar-to-steam generator based on easily available and massively produced commercial materials, such as activated carbon (AC), along with a simple filter paper and styrofoam *via* a vacuum-induced filtration method and industrially used spray coating method. The photothermal layer of AC was separated from the insulating styrofoam by the filter paper that supplies water to the photothermal layer. A sophisticated and complicated method to generate monolithic open macropore channels is not necessary in the method because intraparticle pores are naturally generated between randomly deposited few micrometer-sized AC particles. We used three commercial AC samples with different physical properties corresponding to particle size, specific surface area, and pore size. The PEI was introduced to improve adhesion properties of AC on the filter paper support and enhance water transport, and this was revealed to enhance light absorption and efficiency of solar-to-steam generation. The outdoor field experiment of steam generation and desalination test exhibited the potential of the practical application of the developed AC-based photothermal layers.

2. Methods and experiments

2.1 Materials

Three types of commercial AC were used as photothermal materials, namely Duksan AC (shortly AC-D, Duksan reagent, Republic of Korea), CEP21KS (AC-C, Power Carbon Technology, Republic of Korea), and YP50F (AC-Y, Kuraray, Japan). The Whatman 42 filter papers (with a diameter of 37 mm, GE Whatman, USA) and A4-sized filter paper (210 × 297 mm, Hyundai Micro, Republic of Korea) were used as the supports for photothermal layers in lab-scale and outdoor experiments, respectively. Pieces of styrofoam (47 × 47 × 5 mm for lab scale and 180 × 270 × 22 mm for outdoor experiments) were used as insulating layers. Polyethyleneimine (PEI, 50 weight%, MW = 750 000 g mol^{-1}) was purchased from Sigma-Aldrich and used without further purifications.

2.2 Preparation of AC-based photothermal layers

For lab-scale experiments, 50 mg of AC powder was dispersed in 5 mL of deionized (DI) water *via* an ultrasonic bath (JAC-5020, KODO, Republic of Korea) at room temperature for 30 min. The AC powders were uniformly deposited on the filter paper by vacuum filtration with a deposition area (or diameter of 3.5 cm) of 9.61 cm^2. With respect to the polymer-treated AC, a predefined amount of PEI solution was dissolved in DI water by stirring for 1 h, and this was followed by mixing AC. Specifically, the sample names of the photothermal layers were chosen based on the brand names of AC. Hence, 'ACLA-D', 'ACLA-C' and 'ACLA-Y' indicate AC of Duksan, CEP21KS, and YP50F, respectively, deposited on filter paper. Specifically, 'ACLA-C_PEI' indicates the sample ACLA-C treated with PEI. Typically, 20 mg mL^{-1} polymer solution was used in experiments unless specified during steam generation experiments. After the deposition of AC on filter papers, samples were dried under ambient conditions. With respect to the outdoor experiments, ACLA-C_PEI ink containing 750 mg of CEP21KS mixed with 20 mg mL^{-1} of PEI in 150 mL of DI water was spray-coated on the A4-sized filter paper *via* a spray gun, and this was further dried in atmospheric conditions.

2.3 Steam generation test

All the lab-scale steam generation experiments were performed in a homemade experimental setup. The setup consisted of an electronic balance to track the mass reduction of bulk water due to steam generation, a solar simulator (PEC-L01, Peccell Technologies, Inc., Japan), and an infrared thermometer camera (FLIR 720001, FLIR C2, USA). The illumination power of solar simulator was adjusted to 1, 2, and 3 sun (1 sun = 1 kW m^{-2}). An infrared camera monitored the temperature increase in real-time during the experiment. After each sample was placed on the styrofoam piece floating on DI water filled in a petri dish, the steam generation test was performed for 60 min under the humidity and temperature conditions corresponding to 40–50% and 24–26 °C, respectively.

The outdoor experiments were performed twice at the playground of Chungnam National University on a sunny day and

a sunny–cloudy day. The solar concentration during outdoor experiments was measured *via* a portable light meter (Quantum/Radiometer/Photometer, LI-250A, LI-COR, USA). It was calibrated *via* a solar simulator and calibrated photovoltaic reference cell (BS-520, Sharp Microelectronics, Japan) and resulted in the linear correlation curve (see in ESI, Fig. S1†). The setup consisted of a styrofoam box (230 × 335 × 50 mm, inner parameters) filled with tap water, an electronic balance, and an infrared thermometer camera. In a manner similar to the case of the lab-scale experiment, a bare filter paper or ACLA-C_PEI was placed on a styrofoam piece. As a control sample, a styrobox was filled with only water, and three setups were collectively monitored.

2.4 Artificial seawater preparation

The steam generation for desalination was conducted using artificial seawater. The artificial seawater was prepared based on a classical recipe by Kester *et al.* with a few modifications.[34] All the chemicals, namely NaCl (11.963 g), NaF (0.0025 g), Na_2SO_4 (2.004 g), KCl (0.3335 g), KBr (0.098 g), H_3BO_3 (0.0026 g), $MgCl_2 \cdot 6H_2O$ (0.0266 g), and $CaCl_2 \cdot 2H_2O$ (0.005 g), were dissolved in 500 mL of DI water. The steam generation was performed in a closed chamber using ACLA-C_PEI under illumination of 3 sun, and the condensed water was collected to measure ionic concentration.

2.5 Material characterizations

The morphological information of the samples was obtained *via* field emission scanning electron microscopy (FE-SEM, Hitachi S-4800, Japan) at the National Nanofab Center, Daejeon, Republic of Korea. The Brunauer–Emmett–Teller (BET) surface areas of the AC samples were determined by nitrogen adsorption measurements at −196 °C (BELSORP MINI II, Japan) under a preheat treatment of 150 °C for 3 h with a vacuum of 10^{-2} kPa. The surface elemental composition of ACLA-C and ACLA-C_PEI layer was analyzed *via* X-ray photoelectron spectroscopy (XPS, MULTILAB 2000, Thermo Fisher Scientific, USA). The ionic concentration of the condensed water obtained after the desalination experiment was analyzed *via* inductively coupled plasma atomic emission spectroscopy (ICP-AES, ELAN DRC II, Perkin Elmer, USA). The light absorption of photothermal layer was measured *via* a diffuse reflectance UV-VIS-NIR spectrophotometer with an integrating sphere (SolidSpec-3700, Shimadzu, Japan). The contact angle measurements were carried out using DSA100B-Basic (KRÜSS, Germany).

3. Results and discussion

Fig. 1a shows photographs of ACLA-C photothermal layer prepared by depositing AC on one side of the filter paper *via* the filtration method. The layer exhibited flexibility. The SEM images show AC granules forming a rough surface on the AC-deposited side (Fig. 1b). The size of AC granules used in the study ranged from 6 to 30 μm (Table S1,† Fig. 1b and S2†). The thickness of AC layers approximately corresponded to 160 μm as shown in the SEM image of cross-sectioned AC layer (Fig. 1b). As shown in Fig. S3 and Table S1,† N_2 adsorption–desorption isotherms reveal that only micropores are developed in AC-C with a BET surface area corresponding to 1723 $m^2\ g^{-1}$ while mesopores are also developed in AC-D and AC-Y. As indicated in previous studies, the essential pore characters of photothermal layers for effective solar-to-steam generation corresponded to macroscopic channels through which water and steam should be transported.[11,18,25] Importantly, intraparticle pores and channels can be naturally formed *via* the random deposition of AC particles, as schematically illustrated. The sizes and shapes of pores and channels are inevitably determined by the morphological specifications of AC particles, and this appears as sufficient for efficient water transport *via* capillary action. The micropores and mesopores can play a crucial role in the adsorption of water molecules and polymers, and this is subsequently discussed in further detail.

As shown in the magnified scheme in Fig. 2a, the photothermal layer is located on an insulating film floating on water, and the filter paper plays the role of water uptake. When the edge of the photothermal layer is in contact with water, it becomes completely wet within 2–3 s. This short wetting time indicates efficient water supply through the photothermal layer, and this is crucial in solar-to-steam generation. The temperature distribution mapped by IR camera revealed increased temperature in the AC-deposited area when compared with that on the water surface, thereby indicating that the main photothermal conversion takes places on the AC-deposited area (Fig. 2b). Additionally, the insulator effectively suppressed heat dissipation towards the bulk water due to extremely low thermal conductivity. In order to evaluate the performance of steam generation *via* photothermal layers, the mass change in the bulk water was measured while the temperature change on the surface of photothermal layer was monitored. We have tested three commercial ACs (AC-D, AC-C, and AC-Y) and could select one AC with the highest solar-to-steam generation efficiency. Fig. 2c shows linear plots of the mass change in bulk water as a function of irradiation time measured under 1 sun irradiance. The highest water evaporation rate was measured as 1.17 kg $m^{-2}\ h^{-1}$ with ACLA-C (Fig. 2c). The water evaporation rate by ACLA-Y and ACLA-D corresponded to 1.11 and 1.09 kg $m^{-2}\ h^{-1}$, respectively. The highest steam generation efficiency of ACLA-C would attribute mainly to the highest photothermal conversion efficiency of AC-C as revealed by time-on-stream profiles of surface temperature (Fig. 2d). Under 1 sun irradiation in wet state, the surface temperature of ACLA-C was the highest, and this was followed by ACLA-Y and ACLA-D (Fig. 2d). The surface temperature of ACLA-C reached approximately 44 °C almost immediately after the irradiation, and it subsequently stabilized (Fig. 2d). Specifically, equilibrium was established between simultaneously occurring processes of absorption of the incident light and heat losses *via* the evaporation of water. In addition, pore structures of ACs could have effects on the solar-to-steam generation efficiency. While macroscopic intraparticle pores play the role of the water transporting channels, micropores could be crucial for forming thin water film on the surface of AC by adsorption of water molecules.[35] Since water evaporation takes place at the interface of photothermal materials, here

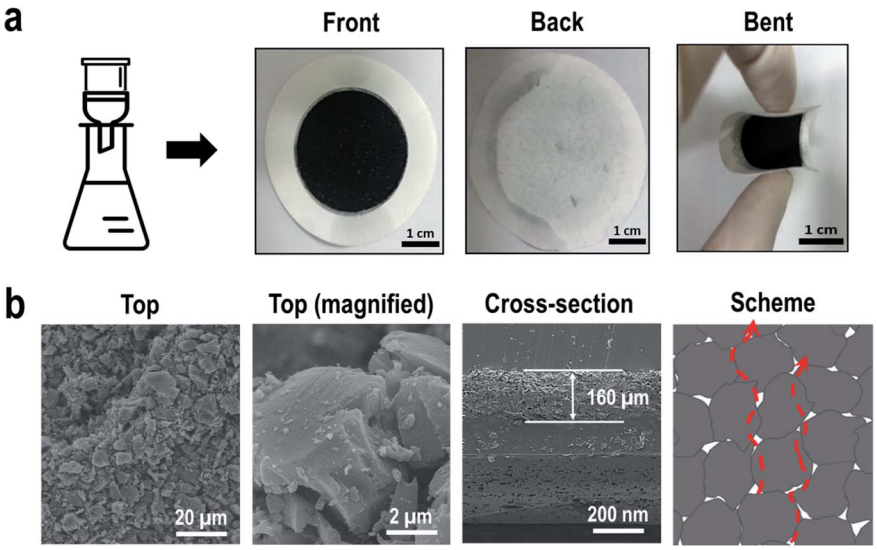

Fig. 1 (a) Photographs of ACLA-C photothermal layer (front, back, and bent) and (b) SEM images of ACLA-C (top, cross-section) with the scheme exhibiting the formation of intraparticle pores through which mass transport occurs.

AC, and thin water film, the development of micropores is advantageous for solar-to-steam generation.[35] Therefore, we speculate that the largest volume of micropores in ACLA-C partly contributes to the highest efficiency of solar-to-steam generation (Fig. S3†).

As shown in Fig. 3a, the water evaporation rate with ACLA-C is dependent on the amount of deposited AC-C per unit area. The highest rate was obtained when the photothermal layer was prepared *via* depositing 52.0 g m^{-2} (thickness of approximately 160 μm) of AC-C on the filter paper. This indicates that excessively thick or thin photothermal layers presumably retard steam generation by insufficient water uptake or by low photothermal conversion. Indeed, improvements in the water wettability of originally hydrophobic AC are essential for

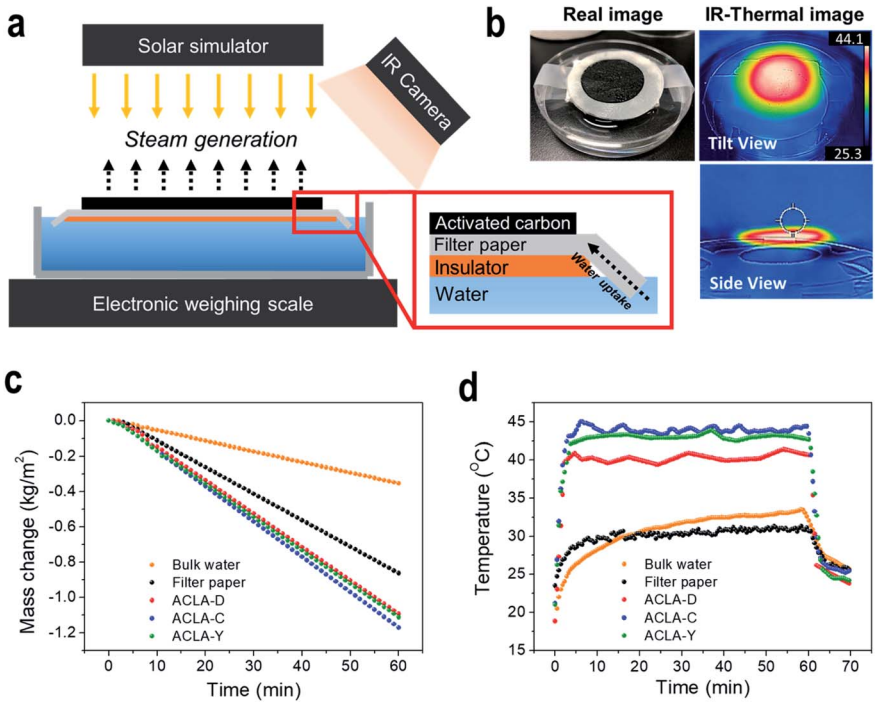

Fig. 2 (a) Schematic illustration of the lab-scaled experimental setup for solar-to-steam generation, (b) real image and IR thermal images of the photothermal layer in the wet condition under 1 sun, (c) mass change profile by solar-to-steam generation for 1 h under 1 sun and, (d) temperature profiles of bulk-water, bare filter paper, and three commercial AC-based photothermal layers during solar-to-steam generation under 1 sun.

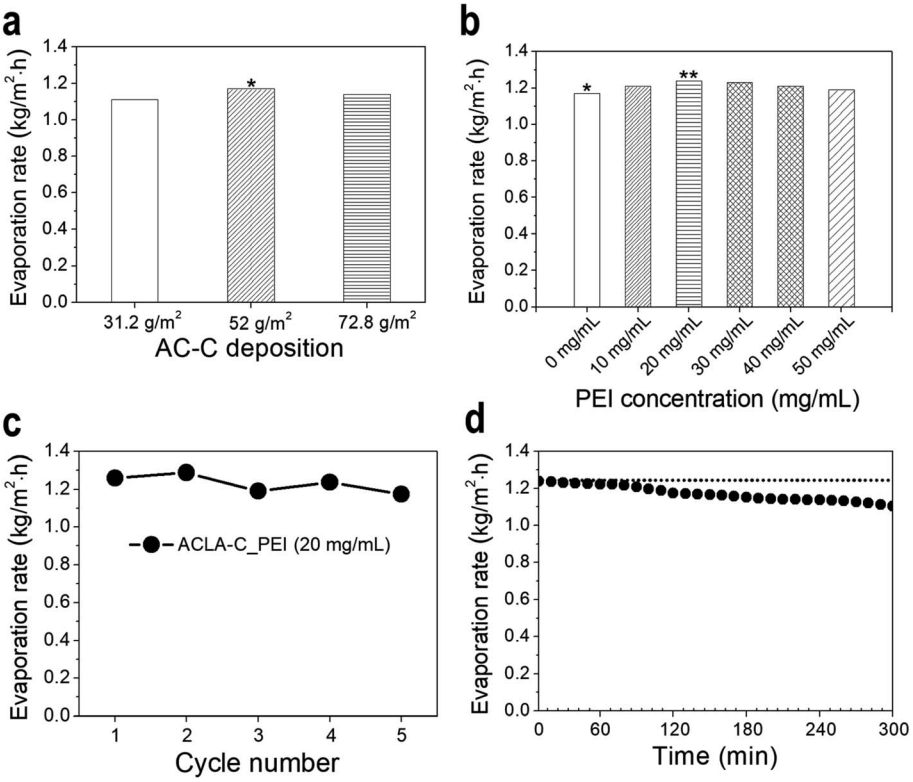

Fig. 3 Mass change in water by solar-to-steam generation for (a) ACLA-C with different loading amounts of AC-C, and (b) ACLA-C_PEI with different concentration of PEI polymer. (c) The cyclic test with drying samples after each measurement using ACLA-C (20 mg mL^{-1}). (d) The time-on-stream evaporation rate of salt water by ACLA-C (20 mg mL^{-1}). All the measurements are performed under the irradiance of 1 sun for 1 h.

effective solar-to-steam generation.[16] This fulfills the requirement of sufficient water supply from bulk water *via* capillary effect throughout intraparticle pores. Thus, water soluble polymers were introduced during the step for deposition of ACs on the filter paper. Specifically, PEI was selected with its high positive charge density provided by abundant primary, secondary, and tertiary amine groups.[36] As shown in Fig. 3b, the water evaporation rate increases after PEI treatment, and 20 mg mL^{-1} of PEI corresponds to the optimal concentration that exhibits the best performance of solar-to-steam generation. The water evaporation rate by ACLA-C_PEI (20 mg mL^{-1}) reached to 1.27 kg m^{-2} h^{-1} under the illumination of 1 sun including the spontaneous evaporation. This corresponds to the photothermal conversion efficiency of 85.66% (see ESI for the detailed evaluation†). The water evaporation rate under 0 sun, namely the spontaneous evaporation, was measured to be 0.16 kg m^{-2} h^{-1}. The water evaporation rate was increased by 3.5 times (enhancement factor, 3.5) in the presence of ACLA-C_PEI. When the PEI concentration exceeds 20 mg mL^{-1}, the water evaporation rate was decreased slightly (Fig. 3b). This is presumably because the polymer molecules block ACLA intraparticle pores due to the swelling effect and result in retarded water uptake and decreased evaporation of water. The cyclic test reveals the durability of ACLA-C_PEI (20 mg mL^{-1}) in the solar-to-steam generation. In spite of the harsh conditions of drying samples after each test, the evaporation rate was not decreased more than 10% up to 5 times (Fig. 3c). The evaporation rate of salt water showed slight decrease (11% for 5 hours) due to the precipitated salt on the surface of ACLA-C_PEI, which could block the incident light and the evaporation of water (Fig. 3d).

Notably, in the dry condition, differences were noted in the surface temperatures of the photothermal layers under 1 sun illumination *via* the PEI treatment. We measured the surface temperatures in dry condition to exclude heat dissipation *via* water evaporation. While the temperature of the cellulose filter paper in dry condition remained in a range similar to that in the case of the wet test (approximately 30 °C, Fig. S4†), the surface temperature of ACLA-C photothermal layers reached approximately 74 °C under 1 sun irradiance as shown in (Fig. 4a). The ACLA-C_PEI exhibited a faster increase in surface temperature than ACLA-C. Light absorption measurement *via* a diffuse reflectance UV-VIS-NIR spectrophotometer with integrating sphere indicated that 91.7% of light was absorbed by ACLA-C over the wavelength range from 240 nm to 2600 nm and that light absorption was enhanced by 4% (95.6%) after PEI treatment (Fig. 4b). This slightly exceeded light absorption by AC fiber felt (94%) which was also applied for solar steam generation.[12] When the wavelength range was restricted to under 1500 nm wherein most solar irradiance is concentrated, 97.0% of light was absorbed by ACLA-C_PEI, and this exceeded light absorption by graphene aerogel (94%) in the same range of wavelength.[16] Given almost no light absorption by PEI itself (Fig. S5†), higher light absorption by ACLA-C after PEI treatment can be attributed to the reduced diffuse reflectance due to two

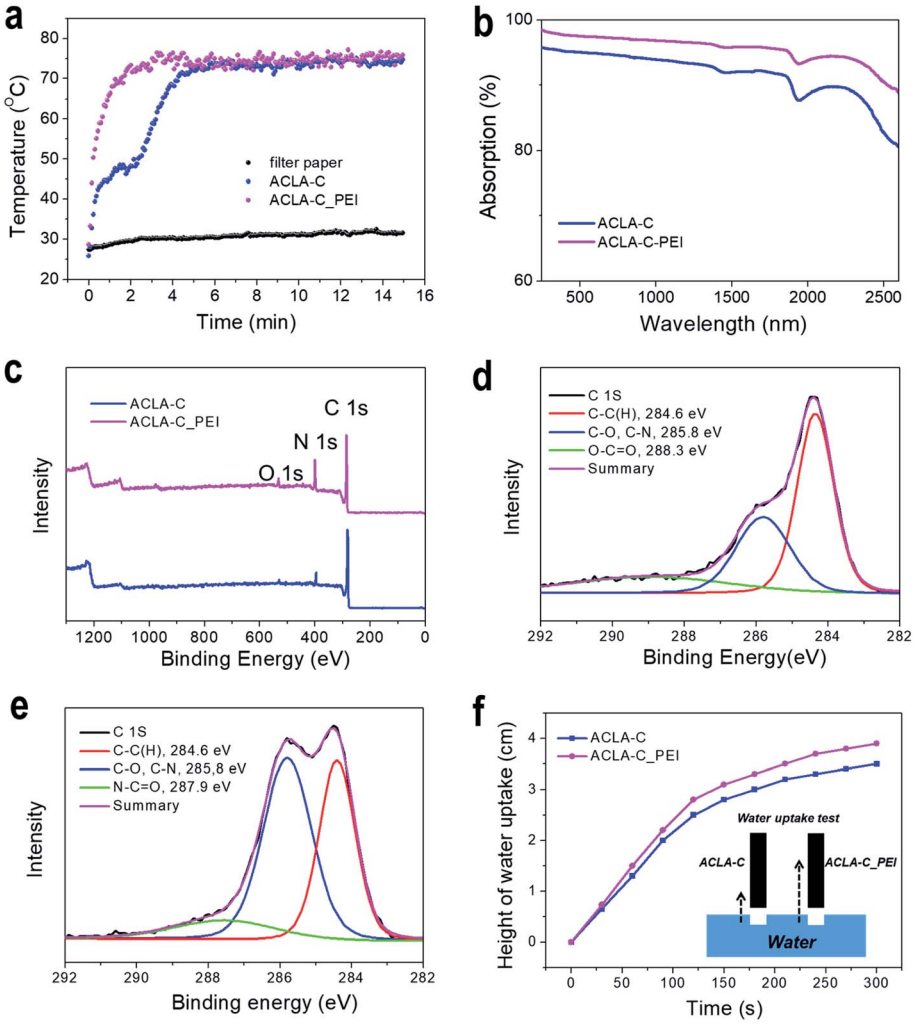

Fig. 4 (a) Surface temperature profiles of ACLA-C and ACLA-C_PEI photothermal layers in dry condition. (b) Absorption spectra of ACLA-C and ACLA-C_PEI measured in dry state. (c) XPS survey scan of ACLA-C and ACLA-C_PEI. High-resolution C 1s spectra of (d) ACLA-C and (e) ACLA-C_PEI, (f) water uptake measurements of ACLA-C and ACLA-C_PEI with respect to time.

factors, namely decrease of light scattering by smoothening of the rough AC surface *via* the PEI coating and reduction in the refractive index difference at air/AC boundary in the presence of the PEI layer with an intermediate refractive index (1.529).

The XPS analysis of ACLA-C and ACLA-C_PEI was performed. The total scan and deconvolutions of C 1s of ACLA-C and ACLA-C_PEI are shown in Fig. 4c–e, respectively. Evidently, ACLA-C_PEI exhibits significant N 1s peak that originated from primary, secondary, and tertiary amine groups. The characteristic peaks of C–C(H) and C–N were observed at binding energies corresponding to 284.6 eV and 285.8 eV, respectively, for both ACLA-C and ACLA-C_PEI (Fig. 4d and e).[37] The PEI-treated sample exhibited a higher C–N signal when compared to the untreated sample, thereby indicating that the PEI was effectively adsorbed on AC-C.[38] The TGA analysis revealed that the amount of absorbed PEI on AC-C corresponded to 4.7 wt% (Fig. S6†). The mesopores and micropores of AC provided abundant adsorption capacity, and it was reported that up to 29.8 wt% of PEI with low molecular number can be impregnated in AC depending on the type of AC.[39] The water wettability of originally hydrophobic AC can be improved *via* the protonation of the adsorbed amine groups. Fig. 4f and S7† show that water uptake and the wettability were enhanced after PEI treatment. The dry ACLA-C (the film coated with AC-C only) is superhydrophobic and even repels water droplets as shown in the Movie S1† and the snapshots of the movie (Fig. S7†). However, once the ACLA-C film got wet, the contact angle was measured to be 18.6°. On the other hand, the surface of ACLA-C_PEI is suberhydrophilic with high wettability (Movie S2 and Fig. S7†). The exact contact angle was not measurable since the water droplet was soaked in the film soon after it spreads on the film. This demonstrates the effect of PEI coating on the surface wettability of ACs. Hence, in conjunction with enhanced light absorption, this may explain the improved solar-to-steam generation after PEI treatment. Furthermore, the PEI treatment increased the adhesion property of AC-C particles in wet state as well as dry state. While the severe detachment of AC-C powders was clearly observed following the bending test of dry

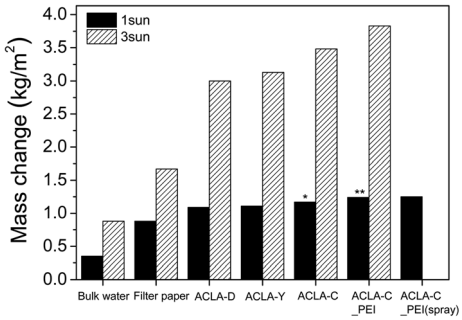

Fig. 5 Summary of water evaporation rates by solar-to-steam generation measured for 1 h under 1 and 3 sun irradiance.

ACLA-C, the PEI-treated ACLA-C layer exhibited comparable robustness under the same test (Fig. S8†). The PEI is a widely used additive to improve wet strength of cellulose in paper industry due to the property of significant absorption on cellulose fibers.[36] Recently, Wang *et al.* used PEI as a cross-linking agent to prepare photothermal layers that are based on graphene oxides and mixed cellulose ester membranes.[40] Improved adhesion between AC-C particles and that between AC-C and filter paper supports this result in robust photothermal layers.

The steam generation performances of ACLA-C and PEI-treated ACLA-C layers under 1 and 3 sun irradiance are summarized in Fig. 5 and Table S2.† The water evaporation rate by ACLA-C_PEI layer under simulated solar irradiation of 1 sun was comparable (1.27 kg m^{-2} h^{-1}) to or exceeded that of previously reported solar-to-steam systems that are mainly based on various nanostructured carbon materials such as graphene, rGO, CNT, or their combinations.[14,15,18] Although the filtration method is simple and cheap, it is restricted to a small scale. For the practical application with large area, we fabricated ACLA-C_PEI(spray) photothermal layer *via* a spray coating method. Its evaporation rate corresponds to 1.24 kg m^{-2} h^{-1}, and this is considerably similar to the performance of ACLA-C_PEI as shown in Fig. 5.

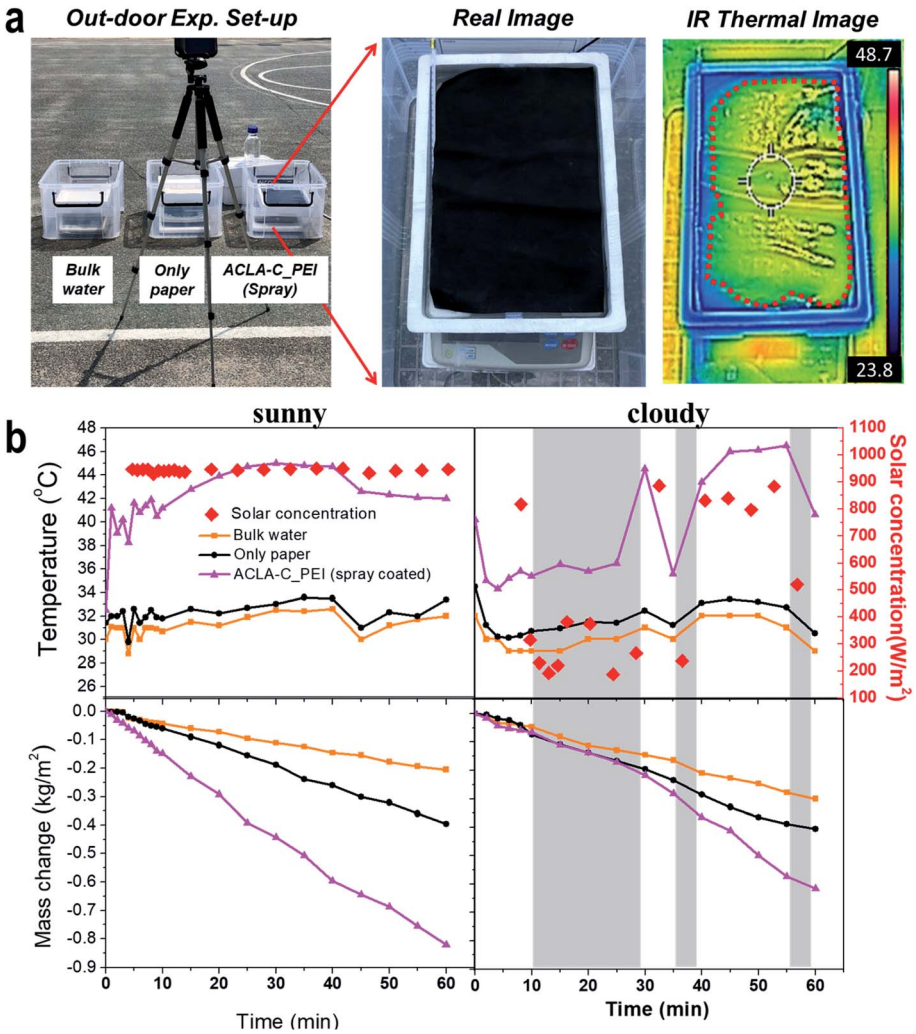

Fig. 6 (a) Outdoor steam generation experiment with real and IR thermal images of large-scale ACLA-C_PEI(spray) photothermal layer, (b) profiles of surface temperature, and mass change in bulk water, water in the presence of filter paper, and ACLA-C_PEI(spray) photothermal layer measured on a sunny and a sunny–cloudy day (experiment date: 05.09.2018, atmospheric conditions: 30 °C, humidity 40%, location: playground of Chungnam National University in Republic of Korea).

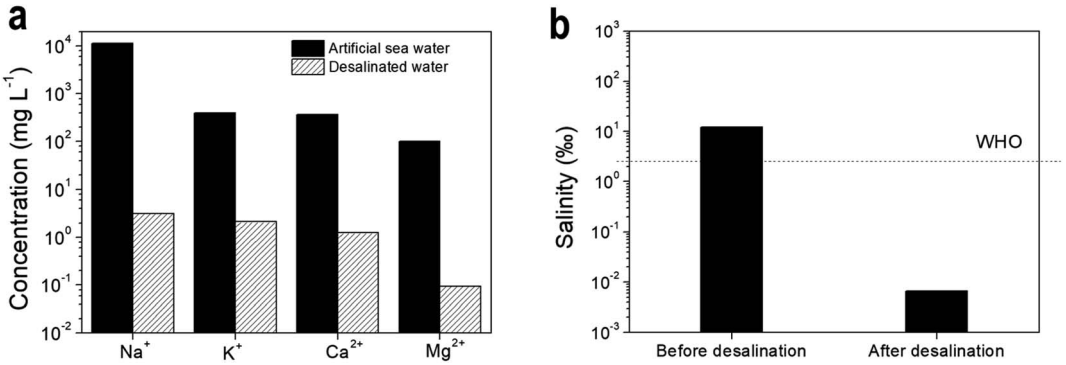

Fig. 7 (a) Concentration of ions in artificial sea water and desalinated water measured by ICP analysis. (b) Salinity data before and after desalination. The dashed line denotes the drinking water salinity standard of World Health Organization (WHO).

Outdoor experiments are performed with an A4-sized ACLA-C_PEI(spray) photothermal layer fabricated by spray coating to evaluate steam generation performance under the real condition of natural sunlight irradiance as shown in Fig. 6. We performed the outdoor tests on a sunny day and a sunny–cloudy day. The mass change in bulk water and that by the filter paper without the photothermal layer were measured under the same conditions for comparison purposes. On a sunny day with approximately 1 sun (1000 W m^{-2}) of illumination, the mass change in water by the ACLA-C_PEI intensively increased and reached a value of 0.82 kg m^{-2} in 1 h, and this was 4.1 and 2.1 times that of bulk water and bare filter paper, respectively (enhancement factor, 4.1). Under cloudy weather, as shown in Fig. 6b with grey mark, it is clearly observed that there is no enhancement in mass change in water by the photothermal layer from 10 to 25 min. When compared to the lab-scale experiment, solar-to-steam generation efficiency in the outdoor was considerably lower in spite of higher enhancement factor. We partly attribute this to poor water uptake. The IR thermal image in Fig. 6a shows the inhomogeneous temperature distribution over the area of A4-sized photothermal layer. As indicated by the red dot line in Fig. 6a, the edge of A4-sized photothermal layer shows the temperature close to that of the bulk water, thereby implying that a proper photothermal conversion-induced interfacial heating is less likely to occur. This demonstrated that uniform supply of water with proper amount to the entire area of the photothermal layer is critical for efficient solar-to-steam generation, and such optimization will be our future study.

We further explored the utilization of ACLA-C_PEI layers for the desalination of seawater. The ion concentration of desalinated water by solar-to-steam generation from artificial seawater is measured by ICP-AES as shown in Fig. 7. When compared with the initial ionic composition of the artificial seawater sample, the concentration of the ions of interest, namely Na^+, K^+, Ca^{2+}, and Mg^{2+} ions, in the desalinated water dropped by 3–4 orders of magnitude (Fig. 7a), and this was comparable to previously reported data.[41,42] Therefore, the salinity after desalination was lower by two orders of magnitude than that of the drinking water quality as prescribed by WHO (Fig. 7b).[42] This demonstrates the potential of AC-based photothermal layers towards solar-to-steam generation for desalination.

4. Conclusion

We devised AC-based photothermal layers that satisfy the main prerequisites, such as high light absorption, monolith open macroporous structure, and hydrophilic surface, for highly efficient solar-to-steam generation. Low cost, upscalability, and simple fabrication constitute important requirements for practical applications toward solar-driven desalination and correspond to the key strengths of the AC-based photothermal layers. The PEI-adsorbed on AC photothermal layers played a crucial role in improving light absorption, water uptake properties, and mechanical robustness. The water evaporation rate by the developed photothermal layers reached 1.27 kg m^{-2} h^{-1} under simulated illumination of 1 sun with an enhancement factor of 3.5. While a considerably reduced rate of 0.85 kg m^{-2} h^{-1} was measured in the outdoor field test using A4-sized photothermal layers under approximately 1 sun illumination, the enhancement factor corresponded to 4.1. The water desalinated from artificial sea water *via* solar-driven steam generation using the AC-based photothermal layers exhibited lower salinity than the criteria of drinking water as prescribed by WHO by 2 orders of magnitude. These suggest that the energy converting system-based on AC photothermal layers is a potential method for performing water purification process at a practical level.

Conflicts of interest

There are no conflicts to declare.

Acknowledgements

This research was supported by a National Research Foundation (NRF) grant (NRF-2020R1A4A2002590). This research was also supported by Korea Electric Power Corporation (grant number: R20XO02-16).

References

1 A. Shah, P. Torres, R. Tscharner, N. Wyrsch and H. Keppner, *Science*, 1999, **285**, 692–698, DOI: 10.1126/science.285.5428.692.

2 A. Kudo and Y. Miseki, *Chem. Soc. Rev.*, 2009, **38**, 253–278, DOI: 10.1039/b800489g.
3 S. Kalogirou, *Prog. Energy Combust. Sci.*, 2005, **31**, 242–281, DOI: 10.1016/j.pecs.2005.03.001.
4 S. Kalogirou, *Solar energy engineering: processes and systems*, Academic Press, Massachusetts, 2nd edn, 2009.
5 O. Neumann, A. S. Urban, J. Day, S. Lal, P. Nordlander and N. J. Halas, *ACS Nano*, 2013, **7**, 42–49, DOI: 10.1021/nn304948h.
6 L. Zhou, Y. Tan, D. Ji, B. Zhu, P. Zhang and J. Xu, *Sci. Adv.*, 2016, **2**, e1501227, DOI: 10.1126/sciadv.1501227.
7 Z. Wang, Y. Liu, P. Tao, Q. Shen, N. Yi and F. Zhang, *Small*, 2014, **10**, 3234–3239, DOI: 10.1002/smll.201401071.
8 Z. Fang, Y. R. Zhen, O. Neumann, A. Polman, F. J. Garcia de Abajo, P. Nordlander and N. J. Halas, *Nano Lett.*, 2013, **13**, 1736–1742, DOI: 10.1021/nl4003238.
9 X. Wu, M. E. Robson, J. L. Phelps, J. S. Tan, B. Shao, G. Owens and H. Xu, *Nano Energy*, 2019, **56**, 708–715.
10 H. Ghasemi, G. Ni, A. M. Marconnet, J. Loomis, S. Yerci and N. Miljkovic, *Nat. Commun.*, 2014, **5**, 4449, DOI: 10.1038/ncomms5449.
11 Y. Ito, Y. Tanabe, J. Han, T. Fujita, K. Tanigaki and M. Chen, *Adv. Mater.*, 2015, **27**, 4302–4307, DOI: 10.1002/adma.201501832.
12 H. Li, Y. He, Y. Hu and X. Wang, *ACS Appl. Mater. Interfaces*, 2018, **10**, 9362–9368, DOI: 10.1021/acsami.7b18071.
13 V. D. Dao and H. S. Choi, *Global Challenges*, 2018, **2**, 1700094, DOI: 10.1002/gch2.201700094.
14 F. Jiang, H. Liu, Y. Li, Y. Kuang, X. Xu and C. Chen, *ACS Appl. Mater. Interfaces*, 2018, **10**, 1104–1112, DOI: 10.1021/acsami.7b15125.
15 Y. Li, T. Gao, Z. Yang, C. Chen, W. Luo and J. Song, *Adv. Mater.*, 2017, **29**, 1700981, DOI: 10.1002/adma.201700981.
16 Y. Fu, G. Wang, X. Ming, X. Liu, B. Hou and T. Mei, *Carbon*, 2018, **130**, 250–256, DOI: 10.1016/j.carbon.2017.12.124.
17 Y. Wang, C. Wang, X. Song, S. K. Megarajan and H. Jiang, *J. Mater. Chem. A*, 2018, **6**, 963–971, DOI: 10.1039/c7ta08972d.
18 L. Shi, Y. Wang, L. Zhang and P. Wang, *J. Mater. Chem. A*, 2017, **5**, 16212–16219, DOI: 10.1039/c6ta09810j.
19 L. Sun, J. Liu, Y. Zhao, J. Xu and Y. Li, *Carbon*, 2019, **145**, 352–358, DOI: 10.1016/j.carbon.2019.01.040.
20 B. Huo, D. Jiang, X. Cao, H. Liang, Z. Liu and C. Li, *Carbon*, 2019, **142**, 13–19, DOI: 10.1016/j.carbon.2018.10.008.
21 H. T. Kieu, K. Zhou and A. W. K. Law, *Appl. Surf. Sci.*, 2019, **488**, 335–342, DOI: 10.1016/j.apsusc.2019.05.247.
22 H. M. Wilson, S. R. AR, T. Garg and N. Jha N, *Appl. Surf. Sci.*, 2019, **487**, 951–961, DOI: 10.1016/j.apsusc.2019.05.080.
23 D. Hao, Y. Yang, B. Xu and Z. Cai, *Appl. Therm. Eng.*, 2018, **141**, 406–412, DOI: 10.1016/j.applthermaleng.2018.05.117.
24 X. Huang, Y. H. Yu, O. L. Llergo, S. M. Marquez and Z. Cheng, *RSC Adv.*, 2017, **7**, 9495–9499, DOI: 10.1039/c6ra26286d.
25 Y. Wang, C. Wang, X. Song, M. Huang, S. K. Megarajan, S. F. Shaukat and H. Jiang, *J. Mater. Chem. A*, 2018, **6**, 9874–9881, DOI: 10.1039/c8ta01469h.
26 K. Bae, B. J. Ku, Y. Kim, A. Mnoyan, K. Lee and K. J. Lee, *ACS Appl. Mater. Interfaces*, 2019, **11**, 4531–4540, DOI: 10.1021/acsami.8b16847.
27 G. Zhu, J. Xu, W. Zhao and F. Huang, *ACS Appl. Mater. Interfaces*, 2016, **8**, 31716–31721, DOI: 10.1021/acsami.6b11466.
28 T. Li, H. Liu, H. Zhao, G. Chen, J. Dai and G. Pastel, *Adv. Funct. Mater.*, 2018, **28**, 1707134, DOI: 10.1002/adfm.201707134.
29 N. Jiang, X. Zhuo and J. Wang, *Chem. Rev.*, 2017, **118**, 3054–3099, DOI: 10.1021/acs.chemrev.7b00252.
30 S. V. Boriskina, H. Ghasemi and G. Chen, *Mater. Today*, 2013, **16**, 375–386, DOI: 10.1016/j.mattod.2013.09.003.
31 Y. Wang, X. Wu, X. Yang, G. Owens and H. Xu, *Nano Energy*, 2020, **78**, 105269.
32 X. Wu, T. Gao and J. Xu, *Sci. Bull.*, 2019, **64**(21), 1625–1633.
33 Y. Wang, X. Wu, B. Shao, X. Yang, G. Owens and H. Xu, *Sci. Bull.*, 2020, **65**(16), 1380–1388.
34 D. R. Kester, I. W. Duedall, D. N. Connors and R. M. Pytkowicz, *Limnol. Oceanogr.*, 1967, **12**, 176–179, DOI: 10.4319/lo.1967.12.1.0176.
35 M. Morciano, M. Fasano, U. Salomov, L. Ventola, E. Chiavazzo and P. Asinari, *Sci. Rep.*, 2017, **7**, 11970.
36 L. Wågberg, *Nord. Pulp Pap. Res. J.*, 2000, **15**, 586–597, DOI: 10.3183/npprj-2000-15-05-p586-597.
37 L. Ma, H. L. Zhuang, S. Wei, K. E. Hendrickson, M. S. Kim and G. Cohn, *ACS Nano*, 2016, **10**, 1050–1059, DOI: 10.1021/acsnano.5b06373.
38 H. J. Kim, I. S. Bae, S. J. Cho, J. H. Boo, B. C. Lee and I. J. Heo, *Nanoscale Res. Lett.*, 2012, **7**, 30, DOI: 10.1186/1556-276X-7-30.
39 C. Y. Yin, M. K. Aroua and W. M. A. Daud, *Mater. Chem. Phys.*, 2008, **112**, 417–422, DOI: 10.1016/j.matchemphys.2008.05.075.
40 G. Wang, Y. Fu, X. Ma, W. Pi, D. Liu and X. Wang, *Carbon*, 2017, **114**, 117–124, DOI: 10.1016/j.carbon.2016.11.071.
41 Q. Chen, Z. Pei, Y. Xu, Z. Li, Y. Yang and Y. Wei, *Chem. Sci.*, 2018, **9**, 623–628, DOI: 10.1039/c7sc02967e.
42 F. Zhao, X. Zhou, Y. Shi, X. Qian, M. Alexander and X. Zhao, *Nat. Nanotechnol.*, 2018, **13**, 489–495, DOI: 10.1038/s41565.

